IEEE Access
Multidisciplinary | Rapid Review | Open Access Journal

SPECIAL SECTION ON GREEN SIGNAL PROCESSING FOR WIRELESS COMMUNICATIONS AND NETWORKING

Received July 29, 2018, accepted August 20, 2018, date of publication August 23, 2018, date of current version September 21, 2018.

Digital Object Identifier 10.1109/ACCESS.2018.2866925

Energy Efficient Space–Time Line Coded Regenerative Two-Way Relay Under Per-Antenna Power Constraints

JINGON JOUNG, (Senior Member, IEEE)
School of Electrical and Electronics Engineering, Chung-Ang University, Seoul 06974, South Korea
e-mail: jgjoung@cau.ac.kr

This research was supported by the National Research Foundation of Korea (NRF) grant funded by the Korea Government (MSIT) (2018R1A4A1023826).

ABSTRACT In multiple-input multiple-output (MIMO) systems, per-antenna power constraint (PAPC) has been considered to enhance the power efficiency of the multiple power amplifiers. Under PAPC, however, a conventional space-division multiple access (SDMA)-based two-way relay (TWR) method suffers a significant bit-error-rate (BER) performance degradation due to the seriously down-scaled transmit power to fulfill the PAPC, which results in energy-efficiency (EE) degradation. In this paper, a new space–time line code (STLC)-based TWR method is proposed to improve the EE. The proposed method can utilize maximum power budget with a low peak-to-average power ratio so that can achieve a better BER performance at the cost of higher power consumption, as verified in numerical simulation results. The benefit of the proposed STLC-based TWR method is justified in terms of EE. The STLC-based TWR system achieves higher EE than the conventional SDMA-based TWR when the maximum transmit power is low, such as a small base station with 23-dBm maximum transmit power. Furthermore, compared with the SDMA-based TWR, the proposed STLC-based TWR can reduce computational complexity by order of magnitude two; therefore, it can be readily extended to a TWR system with a large number of antennas, e.g., a massive MIMO system, which is one of the promising candidates for 5G communications.

INDEX TERMS Energy efficiency, peak-to-average power ratio, per-antenna power constraint, space-division multiple access, space-time line code, two-way relay.

I. INTRODUCTION

Multiple-input multiple-output (MIMO) two-way relay (TWR) system effectively supports data exchange between two source nodes (SNs) within two phases. Various TWR precoders adapted by channel conditions have been rigorously studied, e.g., zero-forcing (ZF)-based spatial-division multiple access (SDMA) precoders in [1]–[4]. In the MIMO TWR precoder design, a sum power constraint (SPC) is typically considered at a relay node (RN), in which the average sum power of all transmit antennas is limited due to the available whole transmit power budget. The SPC allows very unbalanced power over the transmit antennas. In other words, the transmit power of certain antennas can be much greater than that of the others, depending on the channel condition, because an SDMA-based precoding matrix is designed based on the MIMO channel matrix. Since the channels vary over time, the SDMA-based TWR signals have a high peak-to-average power ratio (PAPR). Here, the power amplifiers (PAs) practically have a limit on the output power i.e., a nonlinear characteristic with a saturation [5]. Thus, severe signal distortion is inevitable [5], [6]. In addition to the PA nonlinearity, several hardware impairments, such as phase noise and I/Q imbalance, were studied for TWR systems [7]. On the other hand, to enhance the power efficiency of the multiple PAs, a per-antenna power constraint (PAPC) (see [8] and the references therein) can be considered in the TWR precoder design. However, the transmit power of SDMA-based TWR signals is significantly scaled down in order to fulfill the PAPC sustaining an orthogonal property of SDMA-based precoding matrix. Therefore, the communication performance is seriously deteriorated when PAPC is involved as reported in [9].

In this paper, to resolve the issues from the inherent nature of high PAPR and significantly down-scaled signals of the SDMA-based TWR system under PAPC, we propose a space-time line code (STLC) based TWR scheme.

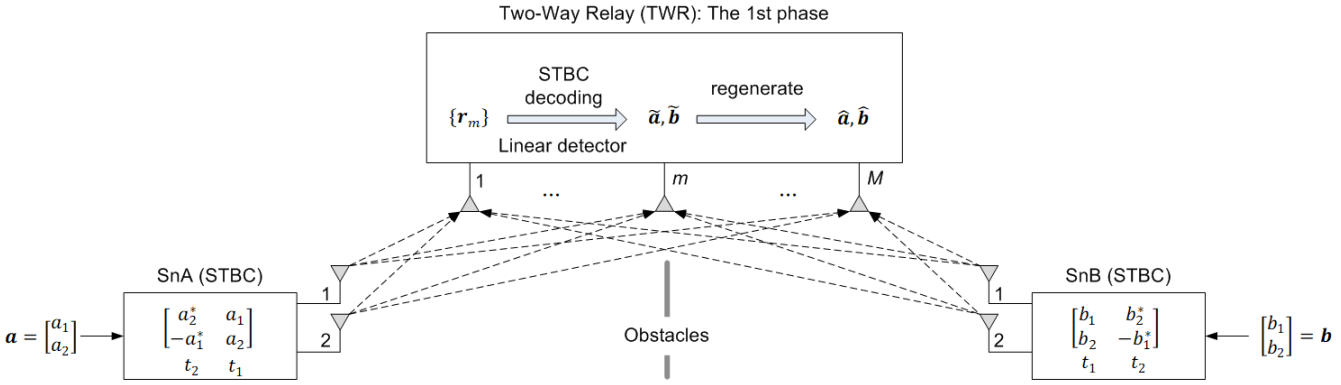

FIGURE 1. Phase-1 transmission from SnA and SnB having two antennas each to a TWR node having M antennas by using an STBC scheme.

The STLC scheme is recently proposed in [10] and [11]. The STLC can provide full rate (i.e., one symbol delivery per transmission) and full-spatial-diversity gain like a space-time block code (STBC) scheme [12]. Moreover, the STLC can be readily applied to a large number of transmit antennas because it can be independently processed for each transmit antenna in parallel [11]. Exploiting the STLC characteristic enabling independent operation per transmit antenna, the PAPC can be directly applied to each STLC signal sustaining the full spatial diversity gain and reducing the PAPR. Furthermore, the STLC-based TWR requires low computational complexity that is linearly proportional to the number of transmit antennas, i.e., $\mathcal{O}(M)$, where M is the number of transmit antennas. On the other hand, the conventional ZF-based SDMA precoders require $\mathcal{O}(M^3)$. Simulation results under the PAPC and the nonlinear PA model verify that the STLC-based TWR can significantly reduce the PAPR by around 5 dB, and at the same time, can improve bit-error-rate (BER) performance, at the cost of more power consumption. To justify the benefit of the proposed STLC-based TWR, energy efficiency (EE) of the TWR systems is evaluated. From the numerical results, it is shown that the proposed STLC-based TWR is more energy efficient than the conventional SDMA-based TWR for a low-power system whose maximum transmit power is low, such as a small base station and a relay station with transmit power up to 23 dBm. To the best of our knowledge, this study is the first attempt to improve TWR performance under PAPC by using an STLC scheme.

A part of the main contributions of this paper are summarized as follows:

- A new STLC-based TWR scheme is proposed for low-complex TWR precoding, spatial diversity gain, and high energy efficiency improvement.
- High PAPR issue of the conventional SDMA-based TWR scheme is investigated.
- Comprehensive experiments are conducted to justify the high energy efficiency of the proposed STLC-based TWR scheme, by comparing to an existing SDMA-based TWR scheme.

The rest of the paper is organized as follows. Section II briefly describes the existing TWR system using STBC and SDMA in the first and second phases, respectively, and examines the high PAPR and significantly down-scaled signal power issues of the conventional SDMA-based TWR scheme. In Section III, an STLC-based TWR scheme is proposed in the second phase and its PAPR and computational complexity are investigated. In Sections IV and V, the performance of BER and EE is evaluated to justify the proposed STLC-based TWR system. Section VI concludes this paper.

Notations: Superscripts T, H, $*$, and -1 denote transposition, Hermitian transposition, complex conjugate, and inversion, respectively, for any scalar, vector, or matrix. The notation $|x|$ and $\|\boldsymbol{x}\|$ denote the absolute value of x and the 2-norm of vector $\boldsymbol{x}$, respectively; $\boldsymbol{I}_m$ and $\boldsymbol{0}_m$ represent an m-by-m identity and zero matrices, respectively; $null(\boldsymbol{X})$ gives the span of nullspace of $\boldsymbol{X}$; and $x \sim \mathcal{CN}(0, \sigma^2)$ means that a complex random variable x conforms to a normal distribution with a zero mean and variance σ^2. E$[x]$ stands for expectation of a random variable x.

II. TWO-WAY RELAY SYSTEM MODEL

Consider a TWR system, in which two SNs A and B (SnA and SnB) with two antennas[1] each exchange their information through a two-way RN with M antennas. Here, no direct link between SnA and SnB is considered due to the obstacles as shown in Fig. 1. The channels from the nth antennas of SnA and SnB to the mth antenna of an RN are denoted by $h_{n,m} = \sqrt{\rho_h}\bar{h}_{n,m}$ and $g_{n,m} = \sqrt{\rho_g}\bar{g}_{n,m}$, respectively, where $n = \{1, 2\}$ and $m = \mathcal{M} = \{1, \ldots, M\}$. Here, ρ_h and ρ_g are the large-scale fading between SnA and RN and between SnB and RN, respectively; and small-scale fading $\bar{h}_{n,m}$ and $\bar{g}_{n,m}$ are independent and identically distributed (i.i.d.) random variables with $\mathcal{CN}(0, 1)$ distribution, i.e., Rayleigh fading channels. Considering a time division duplex TWR system, the channels from SNs to RN and from RN to SNs are assumed

[1]This configuration is merely for the simple description of a spatial-diversity transceiver. For the SNs with more than two antennas, the non-orthogonal STBC and STLC schemes can be applied with a rate lower than one during the first and second phases, respectively.

to be symmetric. To obtain full channel state information (CSI), a typical channel estimation method that uses time-orthogonal training sequences/pilots is considered. Here, SN requires at least M-time slots to estimate the channels from RN to SN, while RN does only four-time slots to estimate the channels from SNs to RN. Considering $M \gg 2$, full CSI assumption is more reasonable at the RN rather than SNs.

A. FIRST PHASE: STBC-BASED TRANSMISSION FROM SOURCE NODES

Following the spatial-diversity transceiver structure introduced in [10], an STBC transmission is considered during the first phase, as shown in Fig. 1. Note that the proposed scheme in this paper later is for TWR in the second phase, and that any type of transmission schemes can be applied to the first phase without affecting the proposed scheme.

For the first time slot t_1, SnA transmits two information symbols $[a_1, a_2]$ to the RN by using two antennas. At the same time, SnB transmits $[b_1, b_2]$ by using two antennas. Subsequently, SnA and SnB transmit $[a_2^*, -a_1^*]$ and $[b_2^*, -b_1^*]$, respectively, at the second time slot t_2. Here, without loss of generality, the average symbol power is assumed to one, i.e., $\mathrm{E}[|a|^2] = \mathrm{E}[|b|^2] = 1$, and the transmit power of SNs is limited per transmit antenna by P_S, i.e., PAPCs [8]. Thus, under the PAPCs, each information symbol is scaled by $\sqrt{P_S}$ before the transmission. The received signals $r_{1,m}$ and $r_{2,m}$ at the mth antenna of the RN at t_1 and t_2, respectively, are then written as follows:

$$\begin{aligned}\begin{bmatrix} r_{1,m} & r_{2,m} \end{bmatrix} &= \begin{bmatrix} h_{1,m} & h_{2,m} \end{bmatrix} \sqrt{P_S} \begin{bmatrix} a_1 & a_2^* \\ a_2 & -a_1^* \end{bmatrix} \\ &\quad + \begin{bmatrix} g_{1,m} & g_{2,m} \end{bmatrix} \sqrt{P_S} \begin{bmatrix} b_1 & b_2^* \\ b_2 & -b_1^* \end{bmatrix} \\ &\quad + \begin{bmatrix} n_{1,m} \\ n_{2,m} \end{bmatrix} \end{aligned} \tag{1}$$

where $n_{t,m}$ is the additive white Gaussian noise (AWGN) at the mth antenna at time slot t with i.i.d. elements, each of which follows a normal distribution $\mathcal{CN}(0, \sigma^2)$.

The RN reconstructs two consecutively received signals $r_{1,m}$ and $r_{2,m}$ at the mth antenna to a vector form as follows:

$$\boldsymbol{r}_m = \begin{bmatrix} r_{1,m} \\ r_{2,m}^* \end{bmatrix} = \sqrt{P_S}\boldsymbol{H}_m\boldsymbol{a} + \sqrt{P_S}\boldsymbol{G}_m\boldsymbol{b} + \boldsymbol{n}_m, \tag{2}$$

where

$$\begin{aligned} \boldsymbol{H}_m &= \begin{bmatrix} h_{1,m} & h_{2,m} \\ -h_{2,m}^* & h_{1,m}^* \end{bmatrix} \\ \boldsymbol{G}_m &= \begin{bmatrix} g_{1,m} & g_{2,m} \\ -g_{2,m}^* & g_{1,m}^* \end{bmatrix}, \\ \boldsymbol{a} &= \begin{bmatrix} a_1 \\ a_2 \end{bmatrix}, \\ \boldsymbol{b} &= \begin{bmatrix} b_1 \\ b_2 \end{bmatrix}, \\ \boldsymbol{n}_m &= \begin{bmatrix} n_{1,m} \\ n_{2,m}^* \end{bmatrix}. \end{aligned}$$

Then, the RN multiplies $\boldsymbol{H}_m^H$ and $\boldsymbol{G}_m^H$ to the $\boldsymbol{r}_m$ in order to detect $[a_1, a_2]$ and $[b_1, b_2]$, respectively, as follows:

$$\boldsymbol{H}_m^H\boldsymbol{r}_m = \gamma_{h,m}\sqrt{P_S}\boldsymbol{a} + \sqrt{P_S}\boldsymbol{H}_m^H\boldsymbol{G}_m\boldsymbol{b} + \boldsymbol{H}_m^H\boldsymbol{n}_m, \tag{3a}$$

$$\boldsymbol{G}_m^H\boldsymbol{r}_m = \sqrt{P_S}\boldsymbol{G}_m^H\boldsymbol{H}_m\boldsymbol{a} + \gamma_{g,m}\sqrt{P_S}\boldsymbol{b} + \boldsymbol{G}_m^H\boldsymbol{n}_m, \tag{3b}$$

where $m = 1, \ldots, M$, and

$$\gamma_{h,m} = |h_{1,m}|^2 + |h_{2,m}|^2, \tag{4a}$$

$$\gamma_{g,m} = |g_{1,m}|^2 + |g_{2,m}|^2. \tag{4b}$$

By summing all the resultant signals through M antennas in (3a), the RN obtains

$$\begin{aligned}\sum_{m\in\mathcal{M}} \boldsymbol{H}_m^H\boldsymbol{r}_m &= \sqrt{P_S}\sum_{m\in\mathcal{M}} \gamma_{h,m}\boldsymbol{a} + \sqrt{P_S}\sum_{m\in\mathcal{M}} \boldsymbol{H}_m^H\boldsymbol{G}_m\boldsymbol{b} \\ &\quad + \sum_{m\in\mathcal{M}} \boldsymbol{H}_m^H\boldsymbol{n}_m, \end{aligned} \tag{5a}$$

$$\begin{aligned}\sum_{m\in\mathcal{M}} \boldsymbol{G}_m^H\boldsymbol{r}_m &= \sqrt{P_S}\sum_{m\in\mathcal{M}} \boldsymbol{G}_m^H\boldsymbol{H}_m\boldsymbol{a} + \sqrt{P_S}\sum_{m\in\mathcal{M}} \gamma_{g,m}\boldsymbol{b} \\ &\quad + \sum_{m\in\mathcal{M}} \boldsymbol{G}_m^H\boldsymbol{n}_m. \end{aligned} \tag{5b}$$

The RN then reconstructs the signals in (5a) as follows:

$$\begin{bmatrix} \sum_{m\in\mathcal{M}} \boldsymbol{H}_m^H\boldsymbol{r}_m \\ \sum_{m\in\mathcal{M}} \boldsymbol{G}_m^H\boldsymbol{r}_m \end{bmatrix} = \boldsymbol{\Gamma}\begin{bmatrix} \boldsymbol{a} \\ \boldsymbol{b} \end{bmatrix} + \begin{bmatrix} \sum_{m\in\mathcal{M}} \boldsymbol{H}_m^H\boldsymbol{n}_m \\ \sum_{m\in\mathcal{M}} \boldsymbol{G}_m^H\boldsymbol{n}_m \end{bmatrix}, \tag{6}$$

where $\boldsymbol{\Gamma}$ is the effective channel matrix from SNs to RN that is written as

$$\boldsymbol{\Gamma} = \begin{bmatrix} \sqrt{P_S}\sum_{m\in\mathcal{M}} \gamma_{h,m}\boldsymbol{I}_2 & \sqrt{P_S}\sum_{m\in\mathcal{M}} \boldsymbol{H}_m^H\boldsymbol{G}_m \\ \sqrt{P_S}\sum_{m\in\mathcal{M}} \boldsymbol{G}_m^H\boldsymbol{H}_m & \sqrt{P_S}\sum_{m\in\mathcal{M}} \gamma_{g,m}\boldsymbol{I}_2 \end{bmatrix}. \tag{7}$$

Applying a linear detector to (6), the RN obtains the estimates of $\boldsymbol{a}$ and $\boldsymbol{b}$ as follows:

$$\begin{aligned}\begin{bmatrix} \tilde{\boldsymbol{a}} \\ \tilde{\boldsymbol{b}} \end{bmatrix} &= \boldsymbol{\Gamma}^{-1}\begin{bmatrix} \sum_{m\in\mathcal{M}} \boldsymbol{H}_m^H\boldsymbol{r}_m \\ \sum_{m\in\mathcal{M}} \boldsymbol{G}_m^H\boldsymbol{r}_m \end{bmatrix} \\ &= \begin{bmatrix} \boldsymbol{a} \\ \boldsymbol{b} \end{bmatrix} + \boldsymbol{\Gamma}^{-1}\begin{bmatrix} \sum_{m\in\mathcal{M}} \boldsymbol{H}_m^H\boldsymbol{n}_m \\ \sum_{m\in\mathcal{M}} \boldsymbol{G}_m^H\boldsymbol{n}_m \end{bmatrix}. \end{aligned} \tag{8}$$

From the estimates in (8), RN detects and regenerates $\hat{\boldsymbol{a}}$ and $\hat{\boldsymbol{b}}$ to relay them to SNs in the second phase.

B. SECOND PHASE: SDMA-BASED TRANSMISSION FROM TWR NODE

The second phase of communication is shown in Fig. 2. A TWR node forwards $\hat{\boldsymbol{a}}$ and $\hat{\boldsymbol{b}}$ to SnB and SnA, respectively, by using a conventional ZF-based SDMA technique [1]–[4], under PAPC by P_R. The channels from an RN to antenna n of SnA and SnB are symmetric to the channels from SNs to RN, and thus, they are represented as the row vectors

$$\boldsymbol{h}_n = [h_{n,1} \cdots h_{n,m} \cdots h_{n,M}]$$

and

$$\boldsymbol{g}_n = [g_{n,1} \cdots g_{n,m} \cdots g_{n,M}],$$

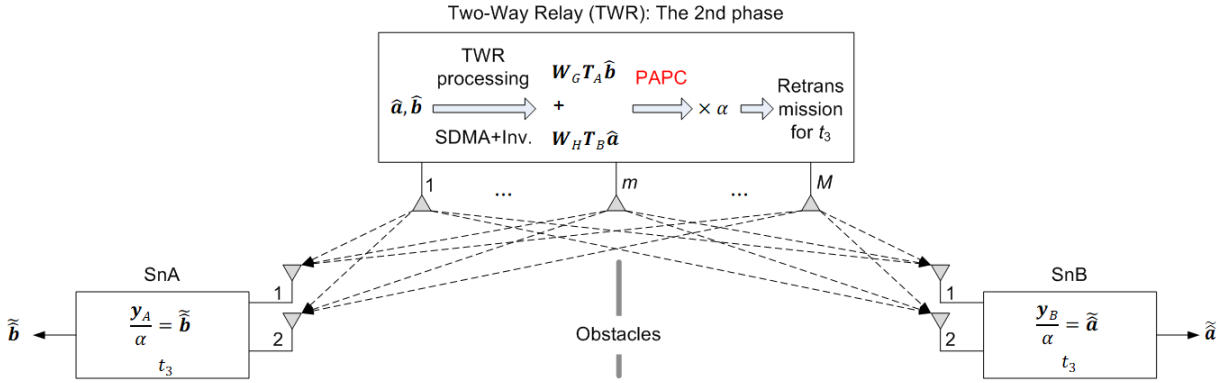

FIGURE 2. Phase-2 transmission from a TWR node to two SNs by using conventional SDMA and channel inversion schemes.

respectively. The channel matrices from RN to SnA and SnB are represented by

$$\boldsymbol{H} = \begin{bmatrix} \boldsymbol{h}_1 \\ \boldsymbol{h}_2 \end{bmatrix} \in \mathbb{C}^{2\times M} \text{ and } \boldsymbol{G} = \begin{bmatrix} \boldsymbol{g}_1 \\ \boldsymbol{g}_2 \end{bmatrix} \in \mathbb{C}^{2\times M},$$

respectively. Full CSI, i.e., $\boldsymbol{H}$ and $\boldsymbol{G}$, is assumed to be available at the RN through the channel estimation during the first phase. The RN forwards $\hat{\boldsymbol{a}}$ and $\hat{\boldsymbol{b}}$ after SDMA and channel inversion precodings. The received signals at SnA and SnB at t_3 are then written as follows:

$$\boldsymbol{y}_A = \boldsymbol{H}\boldsymbol{D}\left(\boldsymbol{W}_G\boldsymbol{T}_A\hat{\boldsymbol{b}} + \boldsymbol{W}_H\boldsymbol{T}_B\hat{\boldsymbol{a}}\right) + \boldsymbol{z}_A, \tag{9a}$$

$$\boldsymbol{y}_B = \boldsymbol{G}\boldsymbol{D}\left(\boldsymbol{W}_G\boldsymbol{T}_A\hat{\boldsymbol{b}} + \boldsymbol{W}_H\boldsymbol{T}_B\hat{\boldsymbol{a}}\right) + \boldsymbol{z}_B, \tag{9b}$$

where $\boldsymbol{D} \in \mathbb{R}^{M\times M}$ is a real-value diagonal matrix for PAPCs; $\boldsymbol{W}_G = null(\boldsymbol{G}) \in \mathbb{C}^{M\times 2}$ and $\boldsymbol{W}_H = null(\boldsymbol{H}) \in \mathbb{C}^{M\times 2}$ are SDMA precoding matrices such that $\boldsymbol{G}\boldsymbol{W}_G = \boldsymbol{0}_2$ and $\boldsymbol{H}\boldsymbol{W}_H = \boldsymbol{0}_2$; $\boldsymbol{T}_A = (\boldsymbol{H}\boldsymbol{W}_G)^{-1} \in \mathbb{C}^{2\times 2}$ and $\boldsymbol{T}_B = (\boldsymbol{G}\boldsymbol{W}_H)^{-1} \in \mathbb{C}^{2\times 2}$ are ZF-based channel inversion precoding matrices; and $\boldsymbol{z}_A \in \mathbb{C}^{2\times 1}$ and $\boldsymbol{z}_B \in \mathbb{C}^{2\times 1}$ are the AWGN vectors at SnA and SnB, respectively. Here, for the ZF-based SDMA precoding, $M \geq 4$. Note that if full CSI is unavail at the SNs when M is very large, a ZF-based channel inversion strategy at RN can be a reasonable approach to eliminate the self-interference. Here, the structure of $\boldsymbol{D}$ should be $\alpha\boldsymbol{I}_M$ to sustain the orthogonal property of SDMA, i.e., $\boldsymbol{G}\boldsymbol{D}\boldsymbol{W}_G = \boldsymbol{0}_2$ and $\boldsymbol{H}\boldsymbol{D}\boldsymbol{W}_H = \boldsymbol{0}_2$. At the same time, $\boldsymbol{D} = \alpha\boldsymbol{I}_M$ fulfills the PAPCs, such that

$$\mathrm{E}\left(\left|\alpha\left[\boldsymbol{W}_G\boldsymbol{T}_A\hat{\boldsymbol{b}} + \boldsymbol{W}_H\boldsymbol{T}_B\hat{\boldsymbol{a}}\right]_m\right|^2\right) \leq P_R, \quad \forall m \in \mathcal{M}, \tag{10}$$

where $[\boldsymbol{x}]_m$ is the mth element of a vector $\boldsymbol{x}$. Therefore, the α is upper bounded as follows:

$$\alpha \leq \alpha_{max} = \min_m \frac{\sqrt{P_R}}{\sqrt{\mathrm{E}\left(\left|\left[\boldsymbol{W}_G\boldsymbol{T}_A\hat{\boldsymbol{b}} + \boldsymbol{W}_H\boldsymbol{T}_B\hat{\boldsymbol{a}}\right]_m\right|^2\right)}}. \tag{11}$$

The PAPC in (11) is a stringent constraint compared to the conventional SPC that is derived as follows:

$$\alpha \leq \frac{\sqrt{MP_R}}{\mathrm{E}\left\|\boldsymbol{W}_G\boldsymbol{T}_A\hat{\boldsymbol{b}} + \boldsymbol{W}_H\boldsymbol{T}_B\hat{\boldsymbol{a}}\right\|}. \tag{12}$$

By virtue of the orthogonal property of SDMA, namely $\boldsymbol{H}\boldsymbol{W}_H = \boldsymbol{0}_2$ and $\boldsymbol{G}\boldsymbol{W}_G = \boldsymbol{0}_2$, the self-interferences disappear from the received signals in (9a) as follows:

$$\begin{aligned} \boldsymbol{y}_A &= \alpha\boldsymbol{H}\left(\boldsymbol{W}_G\boldsymbol{T}_A\hat{\boldsymbol{b}} + \boldsymbol{W}_H\boldsymbol{T}_B\hat{\boldsymbol{a}}\right) + \boldsymbol{z}_A && \text{(13a)} \\ &= \alpha\boldsymbol{H}\boldsymbol{W}_G\boldsymbol{T}_A\hat{\boldsymbol{b}} + \boldsymbol{z}_A && \text{(13b)} \\ &= \alpha\hat{\boldsymbol{b}} + \boldsymbol{z}_A, && \text{(13c)} \\ \boldsymbol{y}_B &= \alpha\boldsymbol{G}\left(\boldsymbol{W}_G\boldsymbol{T}_A\hat{\boldsymbol{b}} + \boldsymbol{W}_H\boldsymbol{T}_B\hat{\boldsymbol{a}}\right) + \boldsymbol{z}_B && \text{(13d)} \\ &= \alpha\boldsymbol{G}\boldsymbol{W}_H\boldsymbol{T}_B\hat{\boldsymbol{a}} + \boldsymbol{z}_B && \text{(13e)} \\ &= \alpha\hat{\boldsymbol{a}} + \boldsymbol{z}_B. && \text{(13f)} \end{aligned}$$

Dividing the received signals in (13a) by α, the SNs obtain the estimates of $\hat{\boldsymbol{a}}$ and $\hat{\boldsymbol{b}}$ as follows:

$$\tilde{\hat{\boldsymbol{a}}} = \hat{\boldsymbol{a}} + \frac{\boldsymbol{z}_B}{\alpha}, \tag{14}$$

$$\tilde{\hat{\boldsymbol{b}}} = \hat{\boldsymbol{b}} + \frac{\boldsymbol{z}_A}{\alpha}. \tag{15}$$

To maximize the SNRs of the received signals in (14), obviously, $\alpha = \alpha_{max}$ and it can be known at all SNs through broadcasting it from RN, which is a marginal signaling overhead.

C. TRANSMIT POWER PER ANTENNA OF SDMA-BASED TWR NODE

In Fig. 3, the transmit power over 10^4 symbols of each antenna of an SDMA-based TWR is shown when $M = 40$ and $P_R = 4$ dBm. As shown, the transmit power across 40 antennas changes significantly. The highly dynamic transmit power across the transmit antennas for one channel realization implies that high PAPR per antenna for varying channels, resulting in the PA impairment due to the nonlinearity of the PA [5]. Furthermore, PAPC suppresses the transmit power exceeding the limit P_R. Thus, if the largest transmit power (i.e., the first antenna in the example in Fig. 3) exceeds the limit, it is scaled down to fulfill the PAPC. Here, the transmit

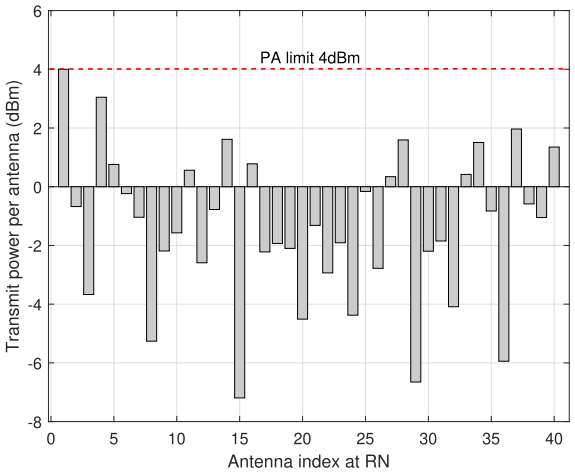

FIGURE 3. Transmit power per antenna of SDMA under PAPC when $M = 40$ and $P_R = 4$ dBm. The transmit power is averaged for 10^4 symbols with one channel realization.

power of all other antennas, even though whose transmit power already meets the PAPC, will be scaled down with the same scaling factor to sustain the SDMA property as stated in the previous subsection. Therefore, the low-power transmission may degrade the communication performance severely. This conjecture is true as verified by simulation in Section IV. To resolve these issues, in the next section, we propose an STLC-based TWR method, which allows for RN to exploit high-power (around its maximum) transmission with low PAPR.

III. PROPOSED STLC-BASED TWR SYSTEM

In this section, we proposed an STLC-based TWR scheme in the second phase communications as shown in Fig. 4. Note that the first phase is the same as that described in Section II.A. In the second phase, the RN encodes $\hat{\boldsymbol{a}}$ and $\hat{\boldsymbol{b}}$, which are obtained through the first phase communications, to an STLC symbol vector as follows:

$$\begin{bmatrix} s^*_{1,m} \\ s_{2,m} \end{bmatrix} = \alpha_m \left(\begin{bmatrix} h_{1,m} & h_{2,m} \\ h^*_{2,m} & -h^*_{1,m} \end{bmatrix} \begin{bmatrix} \hat{b}^*_1 \\ \hat{b}_2 \end{bmatrix} + \begin{bmatrix} g_{1,m} & g_{2,m} \\ g^*_{2,m} & -g^*_{1,m} \end{bmatrix} \begin{bmatrix} \hat{a}^*_1 \\ \hat{a}_2 \end{bmatrix} \right), \quad (16)$$

where $s_{t,m}$ is the STLC symbol that is transmitted through the mth transmit antenna at time $t \in \{t_3 = 1, t_4 = 2\}$, and α_m is a scaling factor obtained as $\alpha_m = \sqrt{P_R}/\sqrt{\gamma_{h,m} + \gamma_{g,m}}$, such that $\mathrm{E}[|\alpha_m s_{t,m}|^2] = P_R$ to satisfy PAPCs. Then, during the second phase, to relay $\hat{\boldsymbol{a}}$ and $\hat{\boldsymbol{b}}$, the RN broadcasts $s_{1,m}$ and $s_{2,m}$ through the mth antenna at the first- and second-time slots, respectively and sequentially. Consequently, the received signals from all M antennas at SnA are written as follows:

$$y_{A,1,1} = \sum_{m\in\mathcal{M}} \Big(h_{1,m}\alpha_m \big((h^*_{1,m}\hat{b}_1 + h^*_{2,m}\hat{b}^*_2) + (g^*_{1,m}\hat{a}_1 + g^*_{2,m}\hat{a}^*_2) \big) \Big) + z_{A,1,1}, \quad (17a)$$

$$y_{A,1,2} = \sum_{m\in\mathcal{M}} \Big(h_{1,m}\alpha_m \big((h^*_{2,m}\hat{b}^*_1 - h^*_{1,m}\hat{b}_2) + (g^*_{2,m}\hat{a}^*_1 - g^*_{1,m}\hat{a}_2) \big) \Big) + z_{A,1,2}, \quad (17b)$$

$$y_{A,2,1} = \sum_{m\in\mathcal{M}} \Big(h_{2,m}\alpha_m \big((h^*_{1,m}\hat{b}_1 + h^*_{2,m}\hat{b}^*_2) + (g^*_{1,m}\hat{a}_1 + g^*_{2,m}\hat{a}^*_2) \big) \Big) + z_{A,2,1}, \quad (17c)$$

$$y_{A,2,2} = \sum_{m\in\mathcal{M}} \Big(h_{2,m}\alpha_m \big((h^*_{2,m}\hat{b}^*_1 - h^*_{1,m}\hat{b}_2) + (g^*_{2,m}\hat{a}^*_1 - g^*_{1,m}\hat{a}_2) \big) \Big) + z_{A,2,2}, \quad (17d)$$

where $y_{A,1,t}$ and $y_{A,2,t}$ are the received signals at the first and second antennas of SnA, respectively, at time slot $t \in \{t_3, t_4\}$, and $z_{A,1,t}$ and $z_{A,2,t}$ are the corresponding AWGNs. Now, SnA combines the received signals, i.e., STLC decoding [10], [11], and then divides the combined signals by the effective channel gain from RN to SnA, that is derived as $\gamma_h = \sum_{m\in\mathcal{M}} \alpha_m \gamma_{h,m}$, to obtain the estimates $\tilde{\hat{b}}_1$ and $\tilde{\hat{b}}_2$ of $\hat{b}_1$ and $\hat{b}_2$ as follows:

$$\begin{aligned} \tilde{\hat{b}}_1 &= \frac{y_{A,1,1} + y^*_{A,2,2}}{\gamma_h} \\ &= \hat{b}_1 + \frac{1}{\gamma_h} \sum_{m\in\mathcal{M}} \Big(\alpha_m \big((h_{1,m}g^*_{1,m} + h^*_{2,m}g_{2,m})\hat{a}_1 \\ &\quad + (h_{1,m}g^*_{2,m} - h^*_{2,m}g_{1,m})\hat{a}^*_2 \big) \Big) + \frac{z_{A,1,1} + z^*_{A,2,2}}{\gamma_h}, \end{aligned} \quad (18a)$$

$$\begin{aligned} \tilde{\hat{b}}_2 &= \frac{-y_{A,1,2} + y^*_{A,2,1}}{\gamma_h} \\ &= \hat{b}_2 + \frac{1}{\gamma_h} \sum_{m\in\mathcal{M}} \Big(\alpha_m \big((-h_{1,m}g^*_{2,m} + h^*_{2,m}g_{1,m})\hat{a}^*_1 \\ &\quad + (h_{1,m}g^*_{1,m} + h^*_{2,m}g_{2,m})\hat{a}_2 \big) \Big) - \frac{z_{A,1,2} - z^*_{A,2,1}}{\gamma_h}. \end{aligned} \quad (18b)$$

In (18a), the effective channel gain γ_h can be readily estimated at the SnA. Here, we note that the self-interferences, which are the second terms in the right-hand side of (18a) and (18b), are difficult to be eliminated at the SNs, because it is difficult to estimate the coupled interference channels without the additional signaling overhead. However, by virtue of the sufficiently large effective channel gain γ_h, the self-interferences can be suppressed as verified in Section IV.

Concurrently, the received signals at SnB are written as follows:

$$y_{B,1,1} = \sum_{m\in\mathcal{M}} \Big(g_{1,m}\alpha_m \big((h^*_{1,m}\hat{b}_1 + h^*_{2,m}\hat{b}^*_2) + (g^*_{1,m}\hat{a}_1 + g^*_{2,m}\hat{a}^*_2) \big) \Big) + z_{B,1,1}, \quad (19a)$$

$$y_{B,1,2} = \sum_{m\in\mathcal{M}} \Big(g_{1,m}\alpha_m \big((h^*_{2,m}\hat{b}^*_1 - h^*_{1,m}\hat{b}_2) + (g^*_{2,m}\hat{a}^*_1 - g^*_{1,m}\hat{a}_2) \big) \Big) + z_{B,1,2}, \quad (19b)$$

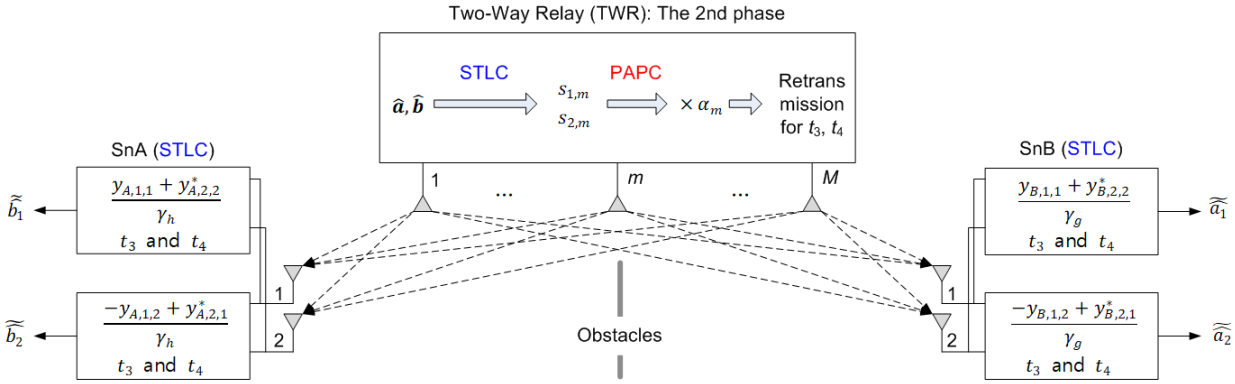

FIGURE 4. Phase-2 transmission from a TWR node to two SNs by using the proposed STLC-based TWR scheme.

$$y_{B,2,1} = \sum_{m\in\mathcal{M}} \Big(g_{2,m}\alpha_m \big((h^*_{1,m}\hat{b}_1 + h^*_{2,m}\hat{b}^*_2) + (g^*_{1,m}\hat{a}_1 + g^*_{2,m}\hat{a}^*_2) \big) \Big) + z_{B,2,1}, \quad (19c)$$

$$y_{B,2,2} = \sum_{m\in\mathcal{M}} \Big(g_{2,m}\alpha_m \big((h^*_{2,m}\hat{b}^*_1 - h^*_{1,m}\hat{b}_2) + (g^*_{2,m}\hat{a}^*_1 - g^*_{1,m}\hat{a}_2) \big) \Big) + z_{B,2,2}, \quad (19d)$$

where $y_{B,1,t}$ and $y_{B,2,t}$ are the received signals at the first and second antennas of SnB, respectively, at time slot $t \in \{t_3, t_4\}$, and $z_{B,1,t}$ and $z_{B,2,t}$ are corresponding AWGN. Following the same procedure as the SnA, the SnB obtains the estimates of $\hat{a}_1$ and $\hat{a}_2$, denoted by $\tilde{\hat{a}}_1$ and $\tilde{\hat{a}}_2$, respectively, as follows:

$$\tilde{\hat{a}}_1 = \frac{y_{B,1,1} + y^*_{B,2,2}}{\gamma_g} = \hat{a}_1 + \frac{1}{\gamma_g}\sum_{m\in\mathcal{M}} \Big(\alpha_m \big((g_{1,m}h^*_{1,m} + g^*_{2,m}h_{2,m})\hat{b}_1 + (g_{1,m}h^*_{2,m} - g^*_{2,m}h_{1,m})\hat{b}^*_2 \big) \Big) + \frac{z_{B,1,1} + z^*_{B,2,2}}{\gamma_g}, \quad (20a)$$

$$\tilde{\hat{a}}_2 = \frac{-y_{B,1,2} + y^*_{B,2,1}}{\gamma_g} = \hat{a}_2 + \frac{1}{\gamma_g}\sum_{m\in\mathcal{M}} \Big(\alpha_m \big((-g_{1,m}h^*_{2,m} + g^*_{2,m}h_{1,m})\hat{b}^*_1 + (g_{1,m}h^*_{1,m} + g^*_{2,m}h_{2,m})\hat{b}_2 \big) \Big) - \frac{z_{B,1,2} - z^*_{B,2,1}}{\gamma_g}, \quad (20b)$$

where $\gamma_g = \sum_{m\in\mathcal{M}} \alpha_m \gamma_{g,m}$ is the effective channel gain from RN to SnB.

Remark 1: The proposed STLC-based TWR method transmits two symbols per transmission (i.e., a_1, a_2, b_1, and b_2 for t_3 and t_4), while the SDMA-based TWR method in Section II.B transmits four symbols per transmission (i.e., a_1, a_2, b_1, and b_2 for t_3). Thus, the spectral efficiency of the proposed STLC-based TWR system is half that of the conventional SDMA-based TWR system. The spectral efficiency decrease of the proposed STCL-based TWR method will be considered for the fair comparison with the SDMA-based TWR method, in Section IV.

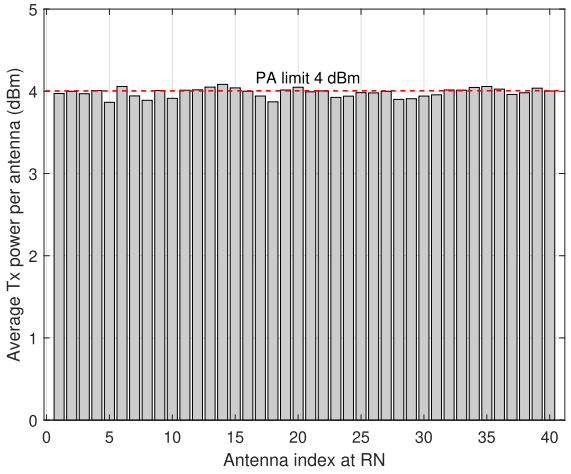

FIGURE 5. Average transmit power per antenna of an STLC-based system with PAPC when $M = 40$ and $P_R = 4$ dBm. The average is performed for 10^4 symbols with one channel realization.

Remark 2: The minimum number of required antennas at TWR is four for the ZF-based SDMA precoding to transmit two symbols per transmission through rank-2 null-space, i.e., $M \geq 4$, while it is only one, i.e., $M \geq 1$, for the proposed STLC-based TWR.

A. TRANSMIT POWER PER ANTENNA OF STLC-BASED TWR NODE

Fig. 5 shows the average transmit power over 10^4 symbols of each antenna of STLC-based TWR node when $M = 40$ and $P_R = 4$ dBm. As observed, the transmit power is almost evenly distributed across 40 antennas under PAPC. From the evenly distributed transit power, lower PAPR and efficient PA operation are expected compared to the SDMA-based TWR system in Section II.C. Fig. 6 shows the complementary cumulative distribution function (CCDF) of PAPR. Here, it is observed that the proposed STLC-based TWR can reduce PAPR more than around 5 dB. Comparing the results

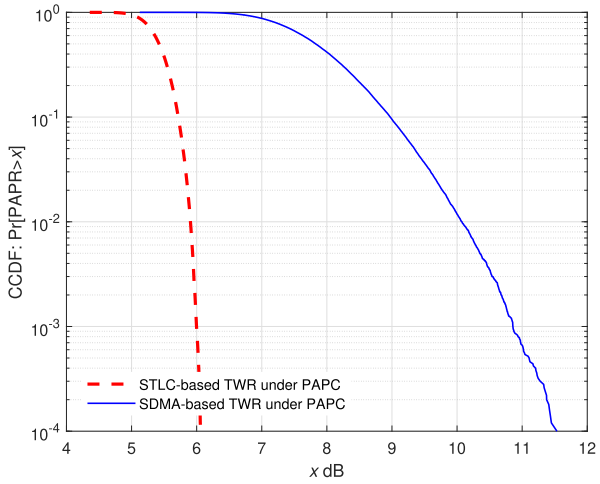

FIGURE 6. PAPR performance comparison between SDMA-based and STLC-based TWR methods when $M = 40$ and $P_R = 4$ dBm.

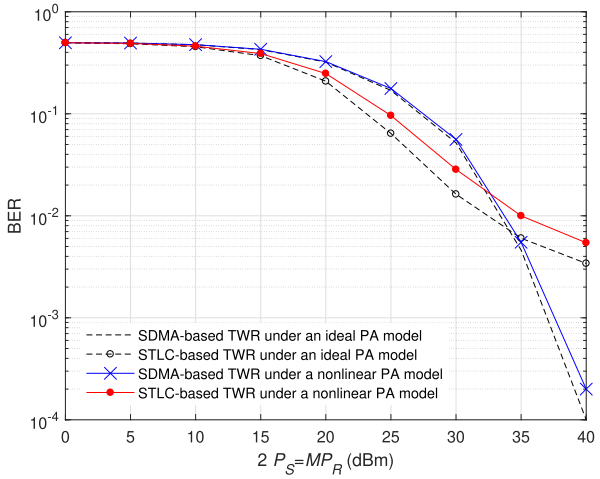

FIGURE 7. BER performance across transmit power when $M = 8$ and $d = 500$ m, under PAPC.

in Figs. 3 and 5, it is clear that the proposed STLC-based TWR transmitter consumes more power than the SDMA-based TWR. Here, it should be reemphasized that the proposed STLC-based scheme fully utilizes the maximum transmit power of PAs efficiently, with low PAPR.

B. COMPLEXITY COMPARISON

Since the first phase is common for the proposed STLC-based and benchmarking SDMA-based schemes, we compare the encoding and decoding complexity in the second phase, which is a complexity bottleneck. The complexity order of the proposed STLC encoding at RN is $\mathcal{O}(M)$ and that of the decoding at SNs is $\mathcal{O}(1)$. Thus, the complexity order of the proposed STLC-based TWR is $\mathcal{O}(M)$. Since the complexity increases linearly proportional to the number of transmit antennas, the proposed STLC-based TWR is applicable to a system with a large number of transmit antennas, e.g., massive MIMO systems. On the other hand, the computational complexity of the SDMA-based scheme is $\mathcal{O}(M^3)$ due to the $null(\cdot)$ operation and inversion of an M-by-2 complex-valued matrix. The significant computational complexity of the conventional SDMA-based TWR hinders the TWR systems from being employed to the MIMO systems with massive antennas.

IV. BER PERFORMANCE EVALUATION AND COMPARISON

Now, the BER performances of the proposed STLC-based and conventional SDMA-based TWR methods are compared under PAPC. For the first phase, 200 quadrature phase-shift keying (QPSK) modulated symbols are transmitted from each SN. In the second phase, for the fair comparison of the STLC- and SDMA-based TWR methods, the data transmission rates are set to be identical to each other. Concretely, the STLC-based TWR forwards the QPSK symbols, while the SDMA-based TWR forwards binary phase-shift keying (BPSK) symbols, for the same transmission time. Note that the spectral efficiency of the STLC-based method is half that of the SDMA-based method as stated in Section III.A. The path loss is modeled as $\rho_h = \rho_g \triangleq \rho = -23.4 + 10\log_{10}(d^{-\mu})$ on dB scale, where G includes the transceiver feeder loss and antenna gains, $d^{-\mu}$ is the path loss for the distance d between nodes (in meter), and μ is a path loss exponent. The small-scale fading is modeled as Rayleigh fading with a zero mean and a unit variance. In our simulation, we set $G = 5$ dB and $\mu = 3.76$. The sum transmit power of SN and that of RN is identical to each other, i.e., $2P_S = MP_R$, and the noise figure is set by -174 dBm.

In Fig. 7, the BER performance is evaluated across transmit power when the number of transmit antennas is eight, i.e., $M = 8$. An ideal PA model and a practical nonlinear PA model are considered. The ideal PA linearly amplifies the input signals for a whole range of transmitting power. The nonlinear PA is modeled as a soft limiter, in which the transmit signal is clipped, such that its power to be equal to the maximum transmit power of the PA if the signal power exceeds the maximum power of the PA [5].

In general, the BER performance of both SDMA- and STLC-based TWR schemes obviously improved as the transmit power budget (i.e., P_S and P_R) increases. Since the proposed STLC-based TWR system performs almost always full-power transmission (see Fig. 5), it is sensitive against the PA models, resulting in nonnegligible performance degradation due to the clipping effect when a nonlinear PA model is involved. However, the proposed STLC-based TWR under PAPC is clearly superior to the SDMA-based TWR scheme, regardless of the PA models. Here, it should be reemphasized that the proposed STLC-based TWR achieves smaller PAPR around 5 dB compared to the SDMA-based TWR system (see Fig. 6). The proposed STLC-based TWR performance is saturated at a high power regime due to the residual self-interferences. The residual self-interference effect can be reduced by increasing the effective channel gain γ_h and γ_g

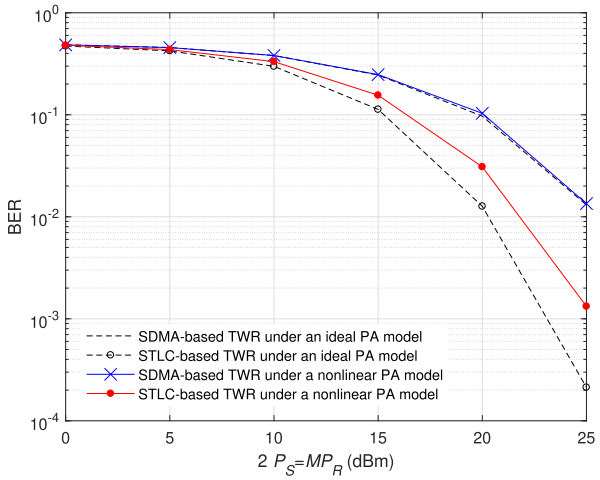

FIGURE 8. BER performance across transmit power when $M = 40$ and $d = 500$ m, under PAPC.

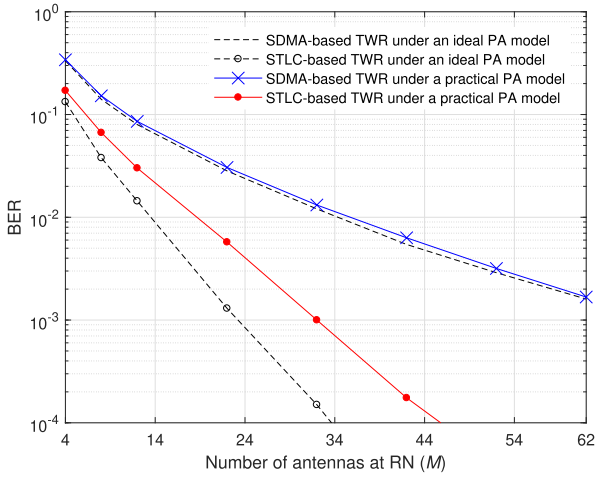

FIGURE 9. BER performance across the number of transmit antennas when $2P_S = MP_R = 26$ dBm and $d = 500$ m, under PAPC.

in (18a) and (20a), respectively, with more transmit antennas as shown in Fig. 8. Here, no saturation is observed up to $MP_R = 40$ dBm, which is omitted in the results. As discussed in Sections II.C and shown in Fig. 3, the transmit power of SDMA-based TWR is significantly scaled down in order to fulfill the PAPC sustaining the orthogonal property of the SDMA-based precoding matrices. Therefore, the SDMA-based TWR systems under PAPC are robust against the PA models. In other words, the SDMA-based TWR signals are linearly amplified. However, the BER performance of the SDMA-based TWR under PAPC is worse than that of the proposed STLC-based TWR scheme due to the inherently low-power SDMA signals. As the transmit power increases, the BER performance of the SDMA-based TWR keeps being improved without saturation since the self-interferences are perfectly canceled out.

In Fig. 9, the BER performance is evaluated for various M. As expected, the performance is improved as M increases due to the suppressed interference (for the STLC-based TWR case) and increased effective channel gain (for both STLC- and SDMA-based TWR cases). The nonlinear PA effect, i.e., performance degradation, increases as M increases for the STLC-based TWR system. However, the proposed STLC-based TWR system outperforms the conventional SDMA-based TWR regardless of M.

V. ENERGY EFFICIENCY COMPARISON

Note that the BER performance improvement of the proposed STLC-based TWR can be achieved at the cost of more power consumption as discussed in Section III.A. Thus, in order to justify the benefit of the proposed STLC-based TWR method, the energy efficiency (EE) should be compared. The EE, denoted by η, is fundamentally defined as a ratio of spectral efficiency (bits/sec/Hz) to the power consumption (Watt) as follows [13]–[15]:

$$\eta = \frac{\text{Spectral Efficiency}}{\text{Power Consumption}} \ \texttt{[bits/sec/Hz/Watt]}, \quad (21)$$

and its unit turns to be bits/Hz/Joule. In the following simulation, η is measured by the ratio of the number of transmit bits reliably relayed without error to the SNs during the second phase to the total power consumption for the retransmissions in the second phase as follows [14], [16]:

$$\eta = \frac{\sum_{t=1}^{T}((1-\epsilon)N)}{\sum_{t=1}^{T} c\sum_{\in\mathcal{M}} P_m + MP_{fix}T} \ \texttt{[bits/Hz/Joule]}, \quad (22)$$

where ϵ is BER for N-bit data transmission for T times; c represents system inefficiency ($c > 1$) that is caused by overhead power consumption at radio frequency circuits; P_m is the transmit power of antenna m; P_{fix} is the fixed power consumption per time slot. In the simulation, $N = 100$ and $T = 10^4$. The parameters related to the power consumption are set as follows [13]–[15]: $c = 5.26$ and $P_{fix} = 45$ dBm. Nonlinear PA is considered and other parameters are the same as the parameters used in Section IV.

In Fig. 10, EE performance (bits/Hz/mJ) across the transmit power of TWR is shown. When the number of transmit antenna increases from eight to 40, the EE decreases because the power consumption increases faster than the increase of the transmission rate. Note that spectral efficiency is a logarithmic function with respect to the transmit power, while the power consumption is linearly proportional to the transmit power. Due to the similar reason, as the transmit power of TWR, i.e., P_R, increases, the EE increases up to a certain point and turns to decrease. It is observed that the EE of the proposed STLC-based TWR is greater than that of the conventional SDMA-based TWR when the transmit power is low, i.e., $MP_R < 32$ dBm, which is clearer when $M = 8$. However, when the transmit power is large, i.e., $MP_R > 32$ dBm, the conventional SDMA-based TWR outperforms the proposed STLC-based TWR method. To further clearly compare the EEs, the EE performance improvement (%) of the proposed STLC-based TWR compared to the

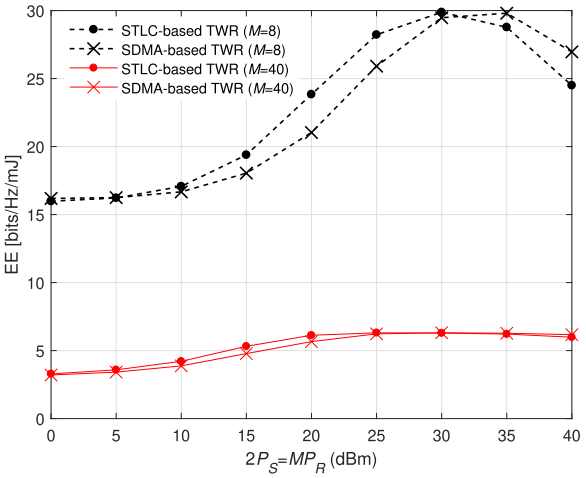

FIGURE 10. EE performance across transmit power P_R of TWR.

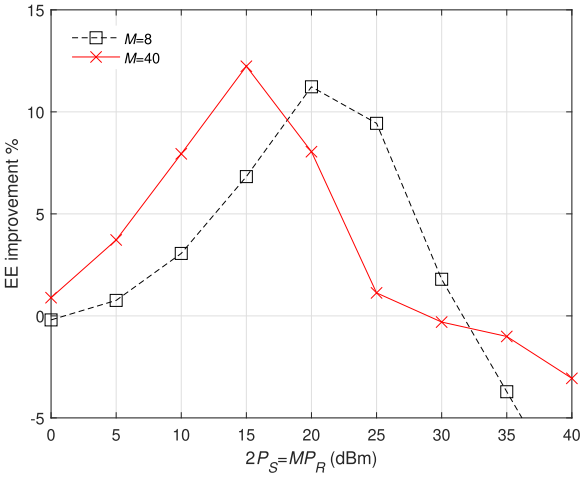

FIGURE 11. EE improvement (%) of the proposed STLC-based TWR system compared to the SDMA-based TWR system across transmit power P_R of TWR.

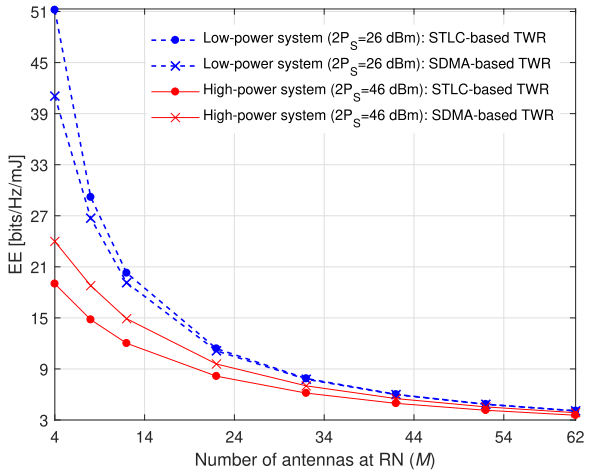

FIGURE 12. EE performance across the number of transmit antennas M.

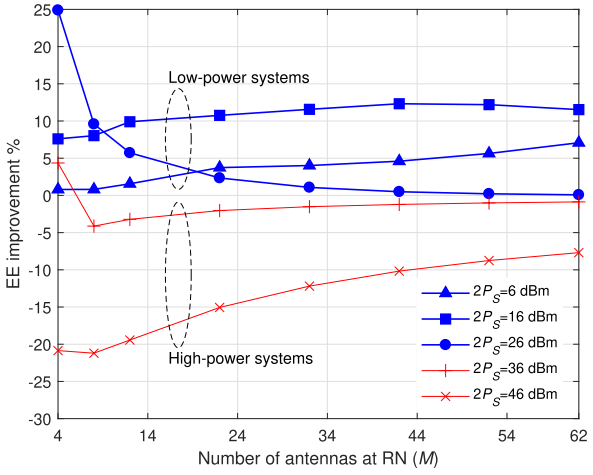

FIGURE 13. EE improvement (%) of the proposed STLC-based TWR system compared to the SDMA-based TWR system across the number of transmit antennas M.

SDMA-based TWR is shown in Fig. 11. From the results, it is clearly observed that the proposed STLC-based TWR has EE benefit when $MP_R < 29$ dBm for $M = 40$ and when $MP_r < 32$ dBm for $M = 8$. The maximum EE improvement is around 12% when $M = 40$.

In Fig. 12, EE performance is evaluated across the number of transmit antennas M when the total transmit power of each node is 23 dBm (i.e., $2P_S = MP_r = 26$ dBm) and 43 dBm (i.e., $2P_S = MP_r = 46$ dBm). The case when the total transmit power is 23 dBm can be interpreted as a case for a *low-power* system including a small base station. On the other hand, the case when the total transmit power is 43 dBm can be interpreted as a case for a *high-power* system including a macro base station.

From the results, it is observed that the EE decreases as M increases owing to the reason discussed in Fig. 10. Clearly, for a low-power system, the proposed STLC-based TWR scheme provides higher EE than the conventional SDMA-based TWR scheme, regardless of the number of transmit antennas. However, the proposed scheme is inferior to the conventional scheme for a high-power system. This result is further clearly observed in Fig. 13. For the low-power systems with $P_S = \{3, 13, 23\}$ dBm, the proposed STLC-based TWR outperforms the conventional SDMA-based TWR in terms of EE.

VI. CONCLUSION

In this paper, an STLC-based TWR method with M antennas is proposed. Under PAPC and with nonlinear PAs, comparing to a conventional SDMA-based TWR system, we verify that the proposed method achieves three merits, at the cost of higher power consumption: i) PAPR reduction by around 5 dB, ii) complexity reduction from $\mathcal{O}(M^3)$ to $\mathcal{O}(M)$, iii) EE improvement for the low-power systems.

REFERENCES

[1] J. Joung and A. H. Sayed, "Multiuser two-way amplify-and-forward relay processing and power control methods for beamforming systems," *IEEE Trans. Signal Process.*, vol. 58, no. 3, pp. 1833–1846, Mar. 2010.

[2] J. Joung and A. H. Sayed, "User selection methods for multiuser two-way relay communications using space division multiple access," *IEEE Trans. Wireless Commun.*, vol. 9, no. 7, pp. 2130–2136, Jul. 2010.
[3] J. Joung, "Beamforming vector design for regenerative wired two-way relay systems," *Electron. Lett.*, vol. 53, no. 9, pp. 596–598, Apr. 2017.
[4] J. Joung and J. Choi, "Linear precoder design for an AF two-way MIMO relay node with no source node precoding," *IEEE Trans. Veh. Technol.*, vol. 66, no. 11, pp. 10526–10531, Nov. 2017.
[5] J. Joung, C. K. Ho, K. Adachi, and S. Sun, "A survey on power-amplifier-centric techniques for spectrum- and energy-efficient wireless communications," *IEEE Commun. Surveys Tuts.*, vol. 17, no. 1, pp. 315–333, 1st Quart., 2014.
[6] S. B. Slimane, "Reducing the peak-to-average power ratio of OFDM signals through precoding," *IEEE Trans. Veh. Technol.*, vol. 56, no. 2, pp. 686–695, Mar. 2017.
[7] K. Guo, D. Guo, and B. Zhang, "Performance analysis of two-way multi-antenna multi-relay networks with hardware impairments," *IEEE Access*, vol. 5, pp. 15971–15980, 2017.
[8] J. Choi, S. Han, and J. Joung, "Low-complexity multiuser MIMO precoder design under per-antenna power constraints," *IEEE Trans. Veh. Technol.*, to be published. [Online]. Available: https://ieeexplore.ieee.org/document/8388257/
[9] A. Wiesel, Y. C. Eldar, and S. Shamai, "Zero-forcing precoding and generalized inverses," *IEEE Trans. Signal Process.*, vol. 56, no. 9, pp. 4409–4418, Sep. 2008.
[10] J. Joung, "Space–time line code," *IEEE Access*, vol. 6, pp. 1023–1041, 2018.
[11] J. Joung, "Space–time line code for massive MIMO and multiuser systems with antenna allocation," *IEEE Access*, vol. 6, pp. 962–979, 2018.
[12] S. M. Alamouti, "A simple transmit diversity technique for wireless communications," *IEEE J. Sel. Areas Commun.*, vol. 16, no. 8, pp. 1451–1458, Oct. 1998.
[13] J. Joung, C. K. Ho, and S. Sun, "Spectral efficiency and energy efficiency of OFDM systems: Impact of power amplifiers and countermeasures," *IEEE J. Sel. Areas Commun.*, vol. 32, no. 2, pp. 208–220, Feb. 2014.
[14] J. Joung and S. Sun, "EMA: Energy-efficiency-aware multiple access," *IEEE Commun. Lett.*, vol. 18, no. 6, pp. 1071–1074, Jun. 2014.
[15] J. Joung, Y. K. Chia, and S. Sun, "Energy-efficient, large-scale distributed-antenna system (L-DAS) for multiple users," *IEEE J. Sel. Topics Signal Process.*, vol. 8, no. 5, pp. 954–965, Oct. 2014.
[16] Y. Sankarasubramaniam, I. F. Akyildiz, and S. W. McLaughlin, "Energy efficiency based packet size optimization in wireless sensor networks," in *Proc. 1st IEEE Int. Workshop Sensor Netw. Protocols Appl.*, Anchorage, AK, USA, May 2003, pp. 1–8.

JINGON JOUNG (S'03–M'07–SM'15) received the B.S. degree in radio communication engineering from Yonsei University, Seoul, South Korea, in 2001, and the M.S. and Ph.D. degrees in electrical engineering and computer science from the Korea Advanced Institute of Science and Technology (KAIST), Daejeon, South Korea, in 2003 and 2007, respectively.

He was a Scientist with the Institute for Infocomm Research, Agency for Science, Technology and Research, Singapore. He joined Chung-Ang University (CAU), Seoul, in 2016. He was a Post-Doctoral Research Scientist with KAIST in 2017 and a Postdoctoral Fellow with the University of California at Los Angeles, Los Angeles, CA, USA, in 2018. He is currently an Assistant Professor with the School of Electrical and Electronics Engineering, CAU, and a Principal Investigator with the Wireless Systems Laboratory. His research activities are in the areas of multiuser systems, multiple-input multiple-output communications, and cooperative systems. His current research area/interests include energy-efficient ICT, IoT, and machine learning algorithms.

Dr. Joung was recognized as the Exemplary Reviewer from the IEEE COMMUNICATIONS LETTERS in 2012 and the IEEE WIRELESS COMMUNICATIONS LETTERS in 2012 and 2013. He was a recipient of the Best Paper Award at the Korean Institute of Communications and Information Sciences conference in 2018 and 2018 and the First Prize at the Intel-ITRC Student Paper Contest in 2006. He has been serving as an Associate Editor for the IEEE TRANSACTIONS VEHICULAR TECHNOLOGY since 2018. He served as a Guest Editor for the IEEE ACCESS for special section—Recent Advanced in Full-Duplex Radios and Networks in 2016. He has been serving on the Editorial Board of the *APSIPA Transactions on Signal and Information Processing* since 2014.